Nox: A Sphinx Mixnet for Anonymous Blockchain Transaction Relay

Jayendra Madaram and Reze Sakiv

Hisoka IO
{jayendra, reze}@hisoka.io

Abstract. Every blockchain interaction leaks network-layer metadata. Zero-knowledge proofs hide transaction content but leave IP addresses, submission timing, and relay payment traces exposed. Mix networks defend against traffic analysis but provide no mechanism for anonymous on-chain interaction. Composing the two as independent layers reintroduces correlation at the boundary: packet timing at the mix network exit correlates with transaction appearance in the mempool, and the relay payment creates an on-chain fingerprint.

Nox is a Sphinx mixnet co-designed with an anonymous transaction relay layer for Ethereum. Exit nodes submit transactions on behalf of anonymous senders. A zero-knowledge gas payment circuit proves relay fee sufficiency without revealing the payer. An execution-hash commitment inside the proof binds each payment to a specific on-chain action. The reply returns through a Single-Use Reply Block (SURB).

Nox applies Reed-Solomon forward error correction to SURB response channels. With 11 data shards and 4 parity shards, multi-fragment delivery rises from 31% to 98% at 10% packet loss without retransmission. FEC has not previously been applied to anonymous reply channels in any mix network. A full open-source implementation is available and deployed on Arbitrum Sepolia.

Keywords: Mix networks, Sphinx, Anonymous communication, Poisson mixing, Forward error correction

1 Introduction

Privacy on public blockchains has received sustained attention. Tornado Cash [22], Railgun [23], and Aztec [24] use zero-knowledge proofs to hide senders, recipients, and amounts. Shielded pools, private transfers, and confidential smart contract execution are now possible on EVM chains. The transaction content problem is, in many practical settings, solved.

The metadata problem is not. Every interaction with a blockchain exposes the client's IP address, the timing of submission, the RPC endpoint queried, and the relay payment trail. Chain-analysis firms operate their own Ethereum nodes and log connection metadata to correlate wallet activity with network addresses. Mempool observers reorder and sandwich transactions for maximal extractable value. A user who submits a shielded transaction through a hosted

RPC provider hides the amount but reveals her IP, her query history, and the exact second she transacted. Paying a relayer to submit on her behalf leaves a fee trace on-chain that narrows the anonymity set. Zero-knowledge proofs do not protect the network layer.

Mix networks do. Chaum introduced the construction [1]. Loopix formalized continuous-time Poisson mixing with cover traffic [3]. Nym [4] and Katzenpost [5] deployed it. Messages traverse intermediaries that strip encryption layers, inject random delays, and add cover traffic to break timing correlation. But composing a mix network and a private transaction system as independent layers reintroduces correlation at the seam: packet timing at the exit correlates with transaction appearance in the mempool, and the relay payment itself creates an on-chain fingerprint. No deployed mix network provides a mechanism for anonymous on-chain interaction.

Two further gaps persist. First, anonymous bidirectional communication via Single-Use Reply Blocks (SURBs) [2] is fragile under multi-fragment responses: a single lost fragment renders the entire response unrecoverable, because SURBs are single-use by construction and cannot be retransmitted. No deployed system addresses this reliability problem. Second, the field suffers from a reproducibility deficit. Nym publishes no performance benchmarks despite operating a production network with over 700 nodes. Katzenpost publishes per-hop microbenchmarks only. Cross-system comparison currently relies on incomplete or self-reported data.

Nox is a Loopix-style Sphinx mix network whose exit nodes double as blockchain transaction relayers. A client encrypts an on-chain operation, together with a zero-knowledge proof of relay fee payment, into a Sphinx packet and submits it to an entry node. The packet traverses three mix layers with Poisson delays and cover traffic. The exit node decrypts the payload, verifies that the relay fee exceeds gas cost, and submits the bound transaction to Ethereum. The reply returns through a SURB. The exit node learns the action it must submit but not the client who requested it. The relay fee is paid from a shielded note pool and verified by a ZK circuit; no on-chain transfer connects the payer to the operation.

This paper makes three contributions.

C1: FEC-enhanced SURB responses. We apply Reed-Solomon forward error correction [11] to SURB response channels. With d=11 data shards and p=4 parity shards, delivery at 10% packet loss rises from 31.0% to 98.2% at a fixed 26.7% bandwidth overhead. We provide a formal recovery model and validate it against 1,000 Monte Carlo trials per loss rate. To our knowledge, this is the first application of FEC to anonymous reply channels in any mix network.

C2: Reproducible benchmark suite. We publish a full-pipeline evaluation covering per-hop Sphinx processing (58.6 μs mean, 2.5$\times$ faster than Katzenpost's equivalent NIKE configuration), end-to-end latency (100.1 ms median under Poisson mixing), sustained throughput (372.3 packets per second), network scaling (5 to 50 nodes), FEC recovery curves, and Shannon entropy analysis. All raw data and generation scripts are published.

C3: Anonymous relay payment. A zero-knowledge gas payment circuit proves relay fee sufficiency without revealing the payer. An execution hash inside the proof binds each payment to a specific on-chain action, preventing proof reuse and front-running. This contribution targets blockchain transaction relay specifically but demonstrates how the mix network can serve applications that require anonymous payment verification.

Section 2 surveys related work. Section 3 defines the threat model. Section 4 presents the system design. Section 5 describes anonymous transaction relay. Section 6 presents the evaluation. Section 7 provides the security analysis. Section 8 discusses limitations. Section 9 concludes.

2 Background and Related Work

2.1 Notation

Table 1. Notation.

Symbol	Meaning
N	Active users
L	Mix layers in the stratified topology
n_i	The i-th mix node on a path
sk_{node}, pk_{eph}	Static secret key, ephemeral public key
s_i	Shared secret between packet and node n_i
ρ, μ, π	Per-hop subkeys: routing, MAC, body
blind	Blinding factor for ephemeral key re-randomization
λ, μ	Poisson rate ($\lambda = 1/\mu$), mean delay
$\lambda_L, \lambda_D, \lambda_P, \lambda_M$	Cover traffic rates: loop, drop, client, mix-node
d, p, r	FEC data shards, parity shards, ratio
ℓ	Per-fragment packet loss rate
$H(X)$	Shannon entropy
f	Fraction of adversarial mix nodes

2.2 Mix Networks

Chaum introduced mix networks as a method for unlinkable communication by routing fixed-size messages through intermediaries that decrypt and reorder them [1]. Kesdogan et al. replaced batch reordering with continuous-time probabilistic delays, where each message is delayed by an independent exponential random interval [7]. Danezis, Dingledine, and Mathewson formalized the Type III anonymous remailer with forward-secure key rotation and directory-based topology [8].

Danezis and Goldberg introduced the Sphinx packet format, which provides per-hop ephemeral key blinding via scalar multiplication with a derived blinding

factor, making the header at hop i cryptographically unlinkable to the header at hop $i{+}1$ under the Decisional Diffie-Hellman (DDH) assumption [2]. Sphinx also defines Single-Use Reply Blocks (SURBs) that allow a responder to send a reply without learning the sender's address. Reply packets are indistinguishable from forward packets on the wire. Scherer and Weis showed that the original DDH-based security proof is insufficient and that the stronger Gap Diffie-Hellman (GDH) assumption is needed [17]. The practical impact is minimal since GDH is believed to hold in the groups used by deployed systems, but the episode illustrates that even well-cited proofs require periodic re-examination.

Piotrowska et al. designed Loopix, whose architectural template Nox follows [3]. Loopix combines Sphinx routing with a stratified topology of configurable depth and continuous-time Poisson mixing modeled as $M/M/\infty$ queuing. Each message is independently delayed by an exponential random variable, and the output of each mix approaches a Poisson process regardless of input burstiness. Loopix introduces four classes of Poisson-distributed cover traffic: loop traffic (λ_L) for volume padding and health monitoring, drop traffic (λ_D) targeting random exit nodes, client payload cover (λ_P) that masks the sending pattern, and mix-node loop traffic (λ_M) generated independently of client activity. The formal privacy analysis uses the Shannon entropy framework of Serjantov and Danezis [9], with per-mix linking probabilities expressed as concrete fractions depending on pool sizes and traffic rates. The Loopix prototype, implemented in Python, reported throughput over 300 messages per second and latency in the order of seconds.

The Nym network extends Loopix into a production deployment with several hundred mix nodes as of early 2026 [4]. Nym adds a Nyx blockchain for decentralized directory services, Coconut credentials [21] for unlinkable threshold-issued bandwidth tokens, and a tokenomic incentive model with Proof-of-Mixing rewards. Despite being the largest deployed mix network, Nym has published no performance benchmarks. Nym's Sphinx implementation contains benchmark scaffolding but no published results.

Katzenpost is a Go-based mix network supporting multiple Sphinx variants: classical NIKE with per-hop blinding factors, KEM variants using hashed ElGamal, and post-quantum hybrids including Xwing (ML-KEM-768 + X25519) [5]. Published per-hop benchmarks report 55.7 μs for X25519 KEM and 144.1 μs for X25519 NIKE. Only Sphinx create/unwrap micro-benchmarks are available; no end-to-end latency or throughput measurements have been published.

Tor uses circuit-based onion routing with immediate forwarding and no mixing [6]. Its design paper explicitly acknowledges the absence of mixing, padding, and traffic shaping. This provides low latency (85 ms median for intra-European circuits per OnionPerf [13]) but leaves Tor vulnerable to traffic analysis attacks that mix networks resist. Tor occupies a fundamentally different point in the design space, prioritizing low latency for interactive use over timing-analysis resistance.

Recent attacks sharpen the threat landscape for all mix networks. Mavroudis and Elahi demonstrated that a Transformer model achieves 95.8% sender identification accuracy against mixnet traffic, with Poisson mixing performing worst

among tested strategies [18]. Oldenburg et al. mounted the first flow-correlation attack on the live Nym network, achieving a true-positive rate of 0.26 at false-positive rate 10^{-2} [19]. Cao and Green exposed vulnerabilities in Nym's reputation system that allow low-stake nodes to damage honest nodes' scores via framing attacks [20]. These results underscore that deployed mix networks face real threats from both passive statistical analysis and active manipulation.

Two lines of work address latency and post-quantum concerns. LAMP introduces geographically proximate mix node routing to reduce inter-hop propagation delay [15]. MOCHA optimizes client anonymity during low-user-count bootstrapping, showing that message-level anonymity metrics overestimate actual client privacy [16]. Both are compatible with Nox's architecture. On the post-quantum front, Outfox proposes a Sphinx variant using ML-KEM-768 that achieves 1 key encapsulation per hop versus 2 scalar multiplications in classical Sphinx [14]. Katzenpost has implemented Outfox variants; integrating post-quantum primitives is future work for Nox.

2.3 Private Blockchain Systems

Tornado Cash demonstrated that zkSNARK Merkle-membership proofs can break the on-chain link between depositors and withdrawers [22]. Users deposit into fixed-denomination pools and later withdraw from a different address by proving Merkle membership via a Groth16 proof without revealing which deposit is theirs. The Tornado Cash Nova extension uses a UTXO model to support arbitrary amounts, removing the denomination constraint. A decentralized relayer registry handles withdrawals, but the on-chain fee trace from relayer to pool remains visible to observers.

Railgun generalizes shielded transfers on EVM chains, supporting arbitrary ERC-20 tokens and private-to-private transfers without unshielding [23]. Railgun routes transactions through the Waku peer-to-peer network, providing partial metadata reduction at the network layer. However, Waku offers no formal mixing guarantees: it provides probabilistic anonymity through message batching but without the timing delays or cover traffic of a dedicated mix network.

Aztec builds a ZK-rollup with programmable private state transitions on its own L2 [24]. Developers designate functions as private (executed client-side) or public (executed by the sequencer). Within the rollup, private functions hide participants and amounts. These systems address content privacy with varying scope, but all three leave the network layer exposed: a user submitting a transaction still reveals her IP address and submission timing to the RPC provider or sequencer.

2.4 Summary

Mix networks protect metadata but offer no mechanism for anonymous on-chain interaction. Private blockchain systems protect content but leak metadata. Composing them as independent layers reintroduces correlation at the boundary. Nox

Table 2. Feature comparison across mix networks and anonymity systems. "N/P" denotes not published.

System	Mix	Cover	SURB	FEC	Anon Pay	Benchmarks
Nox	✓	✓	✓	✓	✓	Full pipeline
Nym	✓	✓	✓	—	—	N/P
Katzenpost	✓	✓	✓	—	—	Micro only
Loopix	✓	✓	✓	—	—	Paper only
Tor	—	—	—	—	—	Full pipeline

is, to our knowledge, the first system that integrates mix routing with FEC-enhanced anonymous reply channels, a zero-knowledge relay-payment mechanism, and a full reproducible benchmark pipeline.

3 Threat Model

3.1 Adversary Capabilities

We consider two adversary classes.

Definition 1 (Global Passive Adversary (GPA)). *Observes all network links, including timing and size of every packet transmitted between any pair of nodes. Cannot modify, delay, inject, or drop packets. The adversary's goal is to link senders to recipients: given an observed message, determine who sent it, who received it, or establish that a particular sender-receiver pair communicated.*

Definition 2 (Limited Active Adversary). *Controls a fraction f of mix nodes, selected uniformly at random. At controlled nodes, the adversary may delay, drop, replay, inject, or reorder packets. It may register additional Sybil nodes subject to the economic cost of staking. The adversary cannot break the Decisional Diffie-Hellman assumption on Curve25519, the collision resistance of Blake3, or the knowledge soundness of UltraPlonk zero-knowledge proofs.*

Blockchain-specific threats. Three attack surfaces extend the standard mix network adversary model.

1. **Relay-payment linkage.** An adversary may correlate the on-chain relay payment (submitted by the exit node) with a message observed exiting the mix network at a particular time. The fee amount and timing narrow the anonymity set. Nox addresses this through zero-knowledge payment proofs that decouple the payer's identity from the on-chain fee transfer.
2. **RPC provider surveillance.** A user's RPC provider observes which smart-contract calls the user submits and when. Even with shielded transaction content, the provider logs the client's IP address and query history. Nox routes all blockchain interaction through the mix network so the RPC provider sees only exit-node IP addresses.

3. **MEV extraction.** Once a transaction reaches the public mempool, searchers may front-run, sandwich, or reorder it for maximal extractable value. Nox does not defend against post-submission MEV: the mix network protects sender identity, not mempool ordering. Integrating private submission channels (e.g., Flashbots Protect or MEV-Share) at the exit node is a natural complement and an area of future work.

3.2 Anonymity Set

Anonymity is measured against two complementary sets. At the network layer, the anonymity set under the GPA comprises all N users who transmitted at least one packet (real or cover) during the mixing window encompassing the target message. With N active users and Poisson mixing with independent per-hop exponential delays, the effective window width depends on the delay parameters $\mu_1, \ldots, \mu_L$ across L layers. Larger delay parameters widen the window and increase the anonymity set at the cost of higher latency.

At the application layer, the anonymity set comprises all unspent notes in the shielded Merkle tree. This set grows monotonically as users deposit into the system. The effective anonymity against a full adversary is the intersection of the two sets: only users whose messages *and* notes are simultaneously active can claim anonymity for their transaction.

3.3 Security Goals

Nox targets five properties:

1. **Sender anonymity.** The adversary cannot determine which user sent a given message with probability significantly greater than random guessing over the network-layer anonymity set, even given full observation of all links.
2. **Receiver anonymity.** The adversary cannot identify the intended recipient of an anonymous reply block before the message is decrypted by the recipient.
3. **Sender-receiver unlinkability.** The adversary observing both ingress and egress messages cannot link a sender message to its corresponding reply with probability greater than the anonymity-set size.
4. **Timing resistance.** The inter-departure times of messages exiting the network are independent of inter-arrival times at the entry, achieved via Poisson mixing and cover traffic.
5. **Payment unlinkability.** The zero-knowledge proof submitted on-chain to authorize relay payment leaks no information about the sender's identity or the message route taken.

3.4 Non-Goals

The following are explicitly outside scope.

- **Long-term intersection attacks.** Users who send messages repeatedly over weeks or months may be deanonymized via passive timing analysis, as demonstrated by Mavroudis and Elahi [18]. Defending against this requires mechanisms outside the mixing protocol itself, such as stronger cover traffic or shorter anonymity windows.
- **Endpoint compromise.** If an attacker compromises a user's device or private keys, plaintext messages and sender identity are directly accessible. We assume clients maintain cryptographic hygiene.
- **Post-quantum adversaries.** The current Sphinx instantiation uses X25519 and BabyJubJub, neither of which is quantum-resistant. Post-quantum Sphinx variants based on ML-KEM exist [14] and represent a natural migration path.
- **Full-layer compromise.** If the adversary controls all nodes in a given layer, it can trivially correlate that layer's inputs and outputs. We assume at least one honest node per layer, the standard assumption for stratified mix networks [10].

4 System Design

4.1 Architecture

Nox follows a stratified topology of Entry, Relay, and Exit nodes matching the Loopix model (Figure 1). Clients construct Sphinx packets locally (the thick client model), selecting a random path through one node from each of $L = 3$ layers. Packets are fixed-size at 32,768 bytes, cryptographically indistinguishable regardless of payload type. Layer assignment is deterministic:

$$\text{layer}(addr) = \text{SHA256}(\text{lowercase}(addr))[0] \bmod L. \tag{1}$$

All clients derive the same assignment from (1) via the on-chain registry, requiring no coordination. For adversarial fraction f and L=3, the probability of full path compromise is f^3. At f=0.2: $0.2^3 = 0.008$ (0.8% of paths).

4.2 Sphinx Packet Format

Packet Structure The routing field holds three 128-byte hop blocks. Each block encodes hop type, next-hop address, and the MAC the next hop verifies. Consumed bytes are replaced with pseudorandom data.

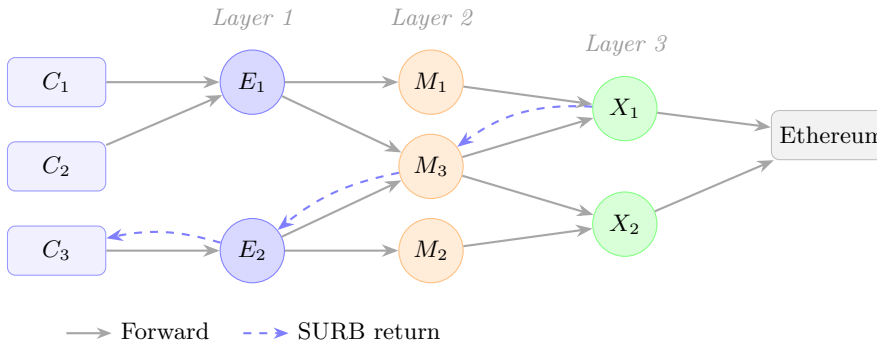

Fig. 1. Stratified 3-layer topology. The bold path shows a forward packet through one node per layer. Dashed arrows show the SURB return path. Each node applies Poisson mixing independently.

Table 3. Packet layout.

Component	**Bytes**	**Contents**
Header	472	Ephemeral key (32), routing (400), MAC (32), PoW (8)
Nonce	12	ChaCha20-Poly1305 AEAD nonce
Ciphertext + tag	32,284	AEAD-encrypted Sphinx body
Total	32,768	

Per-Hop Processing Six operations are performed at each node. Let pk_{eph} denote the ephemeral public key in the header and sk_{node} the processing node's static X25519 secret key.

Step 1. Compute the shared secret via ECDH:

$$s = \text{X25519}(sk_{\text{node}}, pk_{\text{eph}}). \tag{2}$$

Step 2. Derive four subkeys from s using domain-separated SHA-256. The separator strings ensure independence across key usages:

$$\begin{aligned} \rho &= \text{SHA256}(\texttt{"rho"} \| s), & \mu &= \text{SHA256}(\texttt{"mu"} \| s), \\ \pi &= \text{SHA256}(\texttt{"pi"} \| s), & \mathit{blind} &= \text{SHA256}(\texttt{"blind"} \| s). \end{aligned} \tag{3}$$

Step 3. Verify the MAC in constant time. Failure causes immediate packet rejection:

$$\text{HMAC-SHA256}(\mu,\ \mathit{routing\_info}) \stackrel{?}{=} \mathit{header.mac}. \tag{4}$$

Step 4. Decrypt routing information using the subkey ρ from (3): $\mathit{routing}' = \text{ChaCha20}(\rho, 0, \mathit{routing\_info})$. A zero nonce is safe because each (s, ρ) pair is unique per packet and hop.

Step 5. Decrypt the body via the Lioness wide-block cipher [12] (Section 4.2) using subkey π from (3):

$$body' = \text{Lioness}^{-1}(\pi, body). \tag{5}$$

Step 6. Re-randomize the ephemeral public key for the next hop using the blinding factor from (3):

$$pk'_{\text{eph}} = blind \cdot pk_{\text{eph}}, \tag{6}$$

where *blind* is interpreted as a Curve25519 scalar. After blinding, the ephemeral key observed by the next hop is unlinkable to the key at the current hop, provided DDH holds on Curve25519.

Lioness A four-round Luby-Rackoff construction producing a strong pseudorandom permutation (SPRP) over the full body width. The body is split into R (32 bytes) and L (remaining). Four sub-keys (k_1, k_2, k_3, k_4) are derived from π via HKDF-SHA256.

$$L \leftarrow L \oplus S(k_2, R), \tag{7}$$
$$R \leftarrow R \oplus H(k_1, L), \tag{8}$$
$$L \leftarrow L \oplus S(k_4, R), \tag{9}$$
$$R \leftarrow R \oplus H(k_3, L). \tag{10}$$

where $S(k, x)$ is a ChaCha20 keystream seeded by k and $H(k, x)$ is SHA-256 keyed with k. Decryption reverses the sequence.

Proposition 1 (SPRP Tagging Resistance). *The four-round Luby-Rackoff construction in equations (7)–(10), instantiated with ChaCha20 and SHA-256 as independent pseudorandom functions, is a strong pseudorandom permutation (SPRP). Under a uniformly random key, no probabilistic polynomial-time adversary can distinguish Lioness from a random permutation or its inverse with non-negligible advantage. In particular, flipping a single ciphertext bit produces a decrypted body in which approximately 50% of bytes differ from the correct plaintext, because each round's output feeds into the next round's input, diffusing modifications across the full body width. An adversary who tags a packet at one controlled hop cannot detect the tag at a later controlled hop if at least one honest hop applies Lioness decryption in between.*

This follows from the classical result of Luby and Rackoff (1988), which shows that four rounds of a balanced Feistel network over pseudorandom functions yield an SPRP. Anderson and Biham [12] instantiated this construction as LION (later Lioness) with a stream cipher and a hash function.

Packet Construction Clients build Sphinx packets from the innermost (exit) hop outward. A single ephemeral X25519 keypair $(sk_{\text{eph}}, pk_{\text{eph}})$ is generated. Shared secrets are computed via successive blinding: the client computes $s_1 = \text{X25519}(sk_{\text{eph}}, pk_1)$, derives $blind_1$ from s_1 per (3), computes the blinded key $pk_{\text{eph}}^{(1)} = blind_1 \cdot pk_{\text{eph}}$, and uses it for $s_2 = \text{X25519}(sk_{\text{eph}} \cdot blind_1, pk_2)$, continuing for each hop. The body is encrypted under three Lioness layers (innermost first). Construction cost scales linearly: 97 μs for 1 hop, 166 μs for 2, 235 μs for 3 (approximately 69 μs per additional hop).

Lemma 1 (Blinding Correctness). *At each hop i, the processing node can derive the same shared secret s_i from the blinded ephemeral key $pk_{eph}^{(i-1)}$ and its own secret key sk_i. Specifically, $X25519(sk_i, pk_{eph}^{(i-1)}) = s_i$ where $pk_{eph}^{(i-1)} = (\prod_{j=1}^{i-1} blind_j) \cdot pk_{eph}$, because the client used the corresponding blinded secret key to compute s_i during construction.*

Proposition 2 (SURB Indistinguishability). *Under the GDH assumption on Curve25519 [17], a SURB response packet is computationally indistinguishable from a forward Sphinx packet. Both are fixed-size (32,768 bytes), both carry an ephemeral public key that is blinded at each hop per (6), and both encrypt the body under Lioness per (5). An adversary observing a packet on any link cannot determine whether it is a forward message or a SURB response without breaking the GDH assumption.*

4.3 Poisson Mixing

Each node samples delay:

$$\delta \sim \text{Exp}(\lambda), \quad f(\delta) = \lambda e^{-\lambda\delta}, \quad \mathbb{E}[\delta] = \mu = 1/\lambda. \tag{11}$$

Proposition 3 (Output Anonymity). *Consider a single mix node modeled as an $M/M/\infty$ queue: packets arrive according to a Poisson process at rate Λ, and each packet is independently delayed by an exponential random variable with mean μ. In steady state, the number of packets in the queue is Poisson-distributed with parameter $\Lambda\mu$, and the output ordering over n queued packets is uniform over all $n!$ permutations. An adversary observing both input and output streams gains no information about which input produced which output beyond what is implied by the pool size.*

Two properties of exponential delays make this effective. The *memoryless property* states that $\Pr[\delta > t+s \mid \delta > t] = \Pr[\delta > s]$ for all $t, s \geq 0$: observing how long a packet has been in the queue reveals nothing about when it will depart. The *superposition property* states that the merged output of independent Poisson processes is also Poisson [7]. Together, these ensure that the output process of each mix node approaches a Poisson process regardless of the input traffic pattern, as long as the input is itself Poisson or can be approximated as such. Cover traffic (λ_L, λ_D) fills gaps in real traffic, ensuring that the aggregate input to each node remains approximately Poisson even during idle periods.

Total delay for a path through L hops each with exponential delay of mean μ:

$$T_{\text{total}} \sim \Gamma(L, \lambda), \quad f(t) = \frac{\lambda^L t^{L-1} e^{-\lambda t}}{(L-1)!}. \tag{12}$$

From (12), the expected total delay is $\mathbb{E}[T_{\text{total}}] = L\mu$. With L=3 and μ=100 ms (a production setting), the expected mixing delay is 300 ms, acceptable for DeFi operations where Ethereum block times are 12 seconds.

Mutual information across L hops:

$$I(\text{in}; \text{out}) \leq \sum_{i=1}^{L} I_i, \quad I_i \to 0 \text{ as } \mu_i \to \infty \text{ or } \Lambda_i \to \infty. \tag{13}$$

Delays are implemented via a timer wheel: packets are inserted with an expiry instant and emitted in expiry order. This bounds the overhead of mixing at high throughput to a single data structure rather than a task per packet.

4.4 Cover Traffic

Two node-initiated types follow Loopix.

Loop cover ($\lambda_L = 0.05$ pps): each node sends packets through the full 3-layer network back to itself. These self-routed packets carry a heartbeat payload and are indistinguishable from real traffic. They maintain a baseline packet rate during idle periods and serve as health probes: if a loop fails to return within its expected timeframe, the originating node flags the path as degraded.

Drop cover ($\lambda_D = 0.05$ pps): each node sends packets to randomly selected exit nodes, which discard them silently. The exit cannot distinguish a real payload from a dummy without inspecting internal structure, which is protected by Sphinx until final decryption. Drop traffic prevents exit-node traffic analysis.

Client-side cover (λ_P): dummy packets at a configurable Poisson rate mask the sending pattern on the client-to-entry link. Protocol support is implemented. Deployment configuration for bandwidth-constrained mobile clients remains open.

Both node-initiated cover streams sample inter-arrival delays from an exponential distribution with the configured rate, so the aggregate output of each node remains Poisson. At default rates, each node generates $(\lambda_L + \lambda_D) \times 32{,}768 = 3{,}277$ bytes per second of cover traffic.

The anonymity trilemma [10] formalizes the constraint: strong anonymity, low bandwidth overhead, and low latency cannot all be achieved simultaneously. Cover traffic rates trade bandwidth for timing resistance.

4.5 SURBs and FEC

SURB Construction A client pre-builds a Sphinx header encoding a return path from the exit node through the mix layers back to the client. The SURB contains four fields: a 16-byte correlation identifier, the pre-built 472-byte Sphinx

header, the multiaddr of the first return-path hop, and a Lioness key structure for payload encryption. On the client side, a corresponding recovery structure holds per-hop decryption keys and the final payload key.

SURB construction uses raw Curve25519 scalar multiplication rather than clamped X25519, because the cumulative blinding factors that accumulate across the return path are incompatible with X25519 clamping. Each successive shared secret is computed with a secret key multiplied by the accumulated product of previous blinding factors.

Each SURB can be used exactly once: reuse would allow an adversary to correlate two responses to the same sender. Clients expecting multiple responses attach multiple SURBs to each forward request.

Response Delivery The exit node pads the response to fixed size using ISO/IEC 7816-4 padding (append `0x80` then `0x00` bytes), encrypts with the SURB's Lioness keys, and encapsulates the ciphertext into the pre-built header. The result is a standard Sphinx packet, indistinguishable from a forward packet. Padding removal at the client is constant-time to avoid leaking payload length.

FEC for SURB Reliability When a response exceeds single-SURB capacity ($\sim$30,699 bytes), it is split across d data shards plus $p = \lceil d \cdot r \rceil$ parity shards using Reed-Solomon over GF(2^8) [11]. Each shard is encapsulated in a separate SURB packet and dispatched independently through the mix network. Any d of $d{+}p$ fragments suffice for reconstruction by the MDS property. The total shard count is bounded at 255 by the field size.

Theorem 1 (FEC Recovery Probability). *Under independent per-fragment loss ℓ:*

$$\Pr[\textit{recovery}] = \sum_{k=0}^{p} \binom{d+p}{k} \ell^k (1-\ell)^{d+p-k}. \tag{14}$$

Proof. Recovery succeeds iff at most p of $d{+}p$ fragments are lost. Each fragment is lost independently with probability ℓ. The count of lost fragments follows Binomial($d{+}p, \ell$). Summing the PMF over $k = 0, \ldots, p$ gives the CDF at p, which is (14). The independence assumption holds when fragment losses are caused by independent node failures, mixing timeouts, or congestion events; correlated loss (e.g., all fragments sharing a path) would require a different model.

Corollary 1. *With d=11, p=4 at ℓ=0.10:*

$$\Pr[\textit{recovery}] = \sum_{k=0}^{4} \binom{15}{k} (0.1)^k (0.9)^{15-k} \approx 0.987. \tag{15}$$

Without FEC: $(0.9)^{11} \approx 0.314$. *The 3.2$\times$ improvement makes multi-fragment SURB responses viable for practical use.*

The bandwidth overhead is $p/(d{+}p) = 4/15 \approx 26.7\%$. A response requiring 11 packets without FEC requires 15 with FEC.

Why Not ARQ Automatic Repeat reQuest is impractical in mix networks for three reasons. First, retransmission round-trips through the mixnet add 100–400 ms per attempt. Second, retransmission requests must themselves be sent anonymously, doubling the failure surface. Third, retransmission patterns constitute a timing side-channel that aids traffic analysis. FEC embeds all redundancy upfront with no feedback channel.

4.6 Replay Protection

An adversary who captures and replays a Sphinx packet could observe where the duplicate is delivered, breaking sender-receiver unlinkability. Each node prevents this by computing a per-packet replay tag:

$$tag = \text{Blake3}(pk_{\text{eph}} \| mac \| nonce). \tag{16}$$

The tag in (16) is unique per (packet, hop) because the ephemeral public key changes at each hop via blinding (6) and the MAC is recomputed over hop-specific routing information. Tags are checked against a rotational Bloom filter with capacity 10^7 entries and target false-positive rate 0.1%. Old filters rotate hourly: the current filter receives all new tags, while the previous filter is consulted but not written to. This two-window design bounds memory at approximately 17 MB per filter (two filters active at any time) while ensuring that legitimate packets near rotation boundaries are not falsely rejected. Tag computation using Blake3 completes in 159 ns, a negligible fraction of the per-hop processing time.

4.7 Proof of Work

Client finds 8-byte nonce such that

$$\text{leading\_zeros}\big(\text{SHA256}(pk_{\text{eph}} \| routing\_info \| mac \| nonce)\big) \geq d_{\text{pow}}. \tag{17}$$

Verification costs a single hash evaluation. Expected construction cost: $2^{d_{\text{pow}}}$ evaluations. Checked at the ingest stage before any expensive cryptographic processing.

4.8 Relay Pipeline

Packet forwarding is organized as four concurrent stages.

1. **Ingest.** Parses the Sphinx header, checks the replay tag against the Bloom filter, verifies proof of work, and forwards valid packets to the worker pool. Bounded-channel backpressure prevents memory exhaustion.
2. **Worker.** N_w parallel workers (defaulting to the CPU core count) perform the six Sphinx operations from Section 4.2. Workers receive packets via a multi-producer, multi-consumer channel for load balancing.

3. **Mix.** Packets enter a priority queue keyed by their sampled Poisson delay from (11). They are emitted in delay-sorted order.
4. **Egress.** Forwards the processed packet to the next hop or dispatches to the exit service.

All stages run as independent concurrent tasks communicating through bounded channels. Pipeline orchestration overhead is below 1% of total per-hop cost (Table 6).

4.9 DoS Defense

Seven layered defenses protect the relay pipeline: (1) proof of work raises the cost of bulk packet injection; (2) tiered rate limits assign peers to trusted (200 pps), unknown (100 pps), and penalized (25 pps) tiers, with demotion on violation; (3) subnet filtering limits connections to 2 per peer and 50 per /24 prefix; (4) graduated IP banning imposes exponentially increasing ban durations; (5) replay detection via the rotational Bloom filter (Section 4.6); (6) fragmentation limits with TTL-based expiration prevent memory exhaustion from incomplete shard sets; and (7) SSRF and DNS rebinding protection at exit nodes.

5 Anonymous Transaction Relay

This section describes an application-layer extension for blockchain transaction relay. The mix network in Section 4 is application-agnostic; the relay payment mechanism below is one possible use.

5.1 Gas Payment Circuit

A zero-knowledge circuit proves that the client possesses a shielded note with sufficient value to cover the relay fee, without revealing the client's identity, the note consumed, or its position in the Merkle tree. The circuit is compiled with Noir [26] and verified on-chain via UltraHonk.

The proof's public outputs include a nullifier (for double-spend prevention), the payment amount and asset, the relayer's address, an execution hash (Section 5.2), and an encrypted change note returning unspent value to the payer. On-chain, the verifier contract checks the nullifier against a spent set, verifies the proof, deposits the fee into a reward pool, and inserts the change note into the shielded tree. No `msg.sender` check is performed; authorization derives entirely from proof validity. The full circuit specification, including the shielded note structure and nullifier derivation, is described in a companion document on the UTXO protocol.

5.2 Intent Binding

The execution hash binds the proof to a specific on-chain action:

$$eh = \text{keccak256}(target \| calldata \| fee) \bmod p_{\text{BN254}}. \tag{18}$$

The execution hash (18) is a public input to the ZK circuit. If an adversary captures the proof in the mempool and attempts to substitute a different target address or calldata, the on-chain verifier rejects the proof because the recomputed execution hash no longer matches the value committed inside the proof. This prevents three attacks: front-running (submitting the user's proof with a different target), parameter substitution (changing the calldata while reusing the proof), and proof reuse (replaying the proof for a different operation).

5.3 On-Chain Infrastructure

Three contracts compose the on-chain layer. A *node registry* tracks lifecycle, staking, and topology; nodes stake ERC-20 tokens at registration, and clients detect stale topology via an XOR fingerprint over registered addresses. A *reward pool* escrows relay payments; relayers claim accumulated balances periodically. A *batch executor* bundles the payment proof and the user's action into a single atomic transaction. If the payment proof is invalid, the entire batch reverts. If the proof is valid but the user's action fails (e.g., due to slippage), the relayer is still paid. Authorization derives from the ZK proof, not from the sender address.

5.4 Economics

Reads (balance queries, state lookups, proof verification) are free. Making reads free maximizes the anonymity set: every client issues reads regardless of whether they intend to transact, and the exit node cannot distinguish preparatory queries from idle browsing.

Writes require gas. The exit node simulates the transaction via `eth_simulateV1`, computes profitability as revenue minus cost (including gas, priority fee, and base fee), and submits only if revenue exceeds cost by at least 10%. A multi-source gas oracle aggregates price feeds to avoid stale pricing.

6 Evaluation

6.1 Setup

All experiments ran on a single machine: AMD Ryzen 7 9800X3D (8 cores, 96 MB L3 cache), 30.2 GB RAM, Ubuntu 24.04.2 LTS (WSL2), Rust 1.94.1 stable. Release builds use link-time optimization, a single codegen unit, and native CPU targeting. Micro-benchmarks use Criterion.rs [25] with a minimum of 100 iterations per sample and statistical significance testing. Integration benchmarks use two custom binaries: *in-process* (all nodes as concurrent tasks in one process) and *multi-process* (each node as a separate OS process). Unless stated otherwise, the default configuration is a stratified 3-hop topology with 1 ms mean Poisson mixing delay, 256-byte payloads in 32 KB Sphinx packets, and at least 200 trials per data point. All benchmark data, chart generation scripts, and benchmark binaries are published for reproducibility.

Table 4. Per-hop processing, Criterion (core crypto). 58.6 μs is the comparison-appropriate scope.

Operation	Mean (μs)	p50 (μs)	Share (%)
ECDH (X25519)	33.5	28.6	57.2
Key blinding	21.6	28.0	36.9
Body decrypt	1.5	1.4	2.6
MAC verify	0.7	0.6	1.2
Routing decrypt	0.5	0.5	0.9
Key derivation	0.4	0.4	0.7
Total	58.6	59.6	100.0

6.2 Micro-Benchmarks

Table 4 and Figure 2 report Criterion micro-benchmarks measuring core cryptographic operations on smaller payloads. ECDH and key blinding (the two elliptic-curve operations) account for 94.1% of per-hop time. All symmetric operations collectively consume under 3.5 μs. This is the fair comparison against Katzenpost, which benchmarks the same scope.

Table 5 reports integration measurements over 1,429 hop samples with full 32,768-byte bodies, where Lioness body decryption dominates. The gap between 58.6 μs (Criterion) and 118.4 μs (integration) is entirely attributable to the four-round Lioness SPRP operating over the full 32 KB body. At 54.8 μs median, this amounts to approximately 1.7 ns per byte, consistent with the combined cost of ChaCha20 and SHA-256 on this microarchitecture. The 2.0× ratio between p99 and median in both configurations reflects cache pressure and OS scheduling jitter under concurrent load.

Table 5. Per-hop processing, integration (1,429 samples, 32 KB Lioness body).

Operation	Mean (μs)	p50 (μs)	p95 (μs)	p99 (μs)
ECDH	35.9	31.6	62.0	63.2
Body (Lioness)	59.3	54.8	107.4	109.8
Blinding	24.1	30.5	60.4	62.2
MAC	0.8	0.7	1.3	1.4
Routing	0.5	0.5	0.9	1.0
Key derive	0.4	0.4	0.7	0.8
Total	121.0	118.4	231.9	239.1

Additional cryptographic primitive benchmarks (Criterion, release mode): X25519 ECDH shared secret 31 μs, Poseidon2 hash (2 inputs) 6.8 μs, BabyJub-

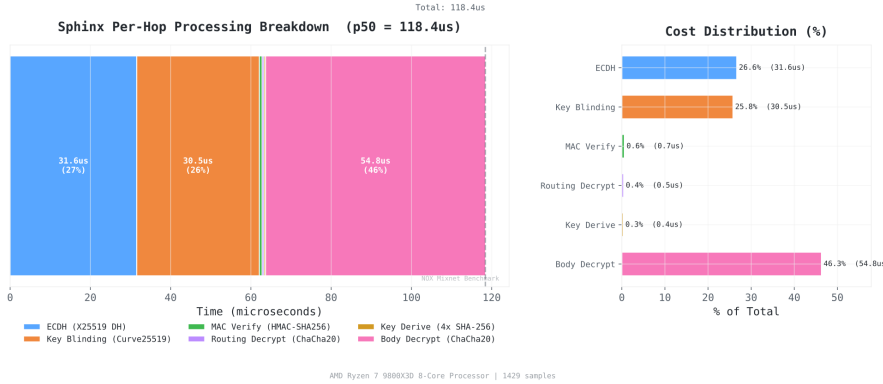

Fig. 2. Per-hop Sphinx processing breakdown. Public-key operations (ECDH + blinding) dominate at 94.1%. Under integration conditions with full 32 KB Lioness body decryption, the body step rises to 46.3% (Table 5).

Table 6. Pipeline stage timings. Orchestration: <1% of per-hop cost.

Stage	Operation	Time
Ingest	Header parse	28 ns
Ingest	Replay tag	161 ns
Ingest	Bloom check	88 ns
Ingest	Full path	714 ns
Worker	Sphinx (forward)	107.6 μs
Worker	Poisson sample	113 ns
Egress	Publish (32 KB)	770 ns
Full	Ingest to egress	108.3 μs

Jub scalar multiplication 3.0 μs, AES-128-CBC encrypt/decrypt 127/58 ns, Blake3 replay tag 159 ns, Sphinx 3-hop construction 235 μs, SURB construction 235 μs, SURB full roundtrip (create + 6 hops) 1.04 ms.

6.3 End-to-End Performance

Table 7 and Figure 3 report end-to-end forward latency. The median of 100.1 ms is dominated by cumulative Poisson mixing delays; cryptographic processing adds less than 0.3 ms per hop. The theoretical mean under Gamma$(3, \lambda)$ at $\lambda = 1$ ms^{-1} is 3 ms; the measured median exceeds this because the benchmark includes event-bus propagation, task scheduling, backpressure, and routing through the full four-stage relay pipeline at each hop. Under production delay parameters ($\mu = 100$ ms), cryptographic overhead ($\approx$0.3 ms per hop) would be negligible compared to the 300 ms expected mixing delay.

Table 7. Latency (5,050 packets, 5 nodes, 3 hops, 1 ms Poisson).

Metric	Value
p50	100.1 ms
p90	224.4 ms
p95	231.9 ms
p99	259.0 ms
Mean	110.7 ms
Std. dev.	92.9 ms
Loss	4.5%

The standard deviation of 92.9 ms reflects the inherent variance of exponential mixing. This variance is not a deficiency; it is the timing obfuscation that resists traffic analysis. The p99 of 259.0 ms is 2.6× the median, consistent with the heavy tail of the Gamma distribution. The 4.5% loss rate results from packets exceeding timeout thresholds due to Poisson-tail outliers.

SURB round-trip times (Figure 4) were measured over 509 successful deliveries (6 total hops: 3 forward + 3 return). The median of 218.8 ms is roughly double the forward latency, as expected for twice the hop count. The p95 of 430.3 ms reflects six convolved exponential delays. The 7.5% loss rate exceeds the forward-only 4.5% because both legs must succeed: with independent 4.5% loss per leg, compound loss approaches $1 - (1 - 0.045)^2 \approx 8.8\%$. The measured 7.5% is slightly lower, likely due to correlated timeout behavior. This elevated loss rate motivates the FEC mechanism in Section 6.4.

Table 8. Throughput sweep. Multi-process: 0% loss at all rates.

Target	Achieved	Loss	Mode	Nodes
1,000	183.4	—	In-proc	5
5,000	276.1	—	In-proc	5
200	126.5	0.0%	Multi	10
500	252.4	0.0%	Multi	10
1,000	372.3	0.0%	Multi	10

Table 8 and Figure 5 show that multi-process mode achieves higher peak throughput (372.3 PPS) than in-process (276.1 PPS) despite more nodes. Distributing across OS processes with independent runtime schedulers avoids single-process contention on the async executor. The 0% loss at all multi-process rates indicates the throughput ceiling has not been reached; the benchmark framework, not the mixnet, is the bottleneck. At 372.3 PPS with 3 hops per packet, each node processes approximately 112 Sphinx operations per second, well within the capacity implied by the 118.4 μs per-hop integration cost (theoretical single-core maximum: ∼8,400 operations per second).

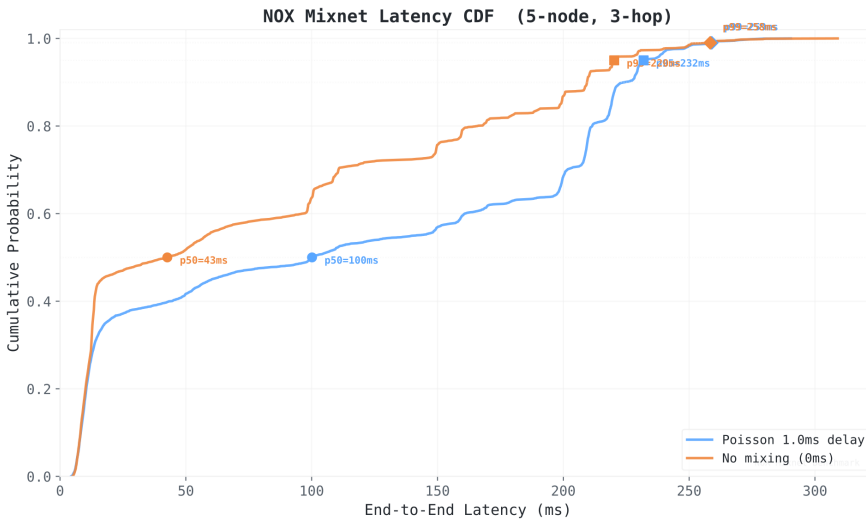

Fig. 3. Latency CDF. The steep rise near the Gamma mode reflects L=3 hop convolution. The tail beyond 200 ms: Poisson outliers.

Table 9. Scaling (multi-process, 200 packets, 1 ms Poisson, 3 hops).

Nodes	PPS	p50 (ms)	σ (ms)	Loss
5	509.7	19.8	50.9	9.1%
10	486.5	52.8	47.6	9.1%
25	365.4	69.5	60.3	9.1%
50	355.3	108.1	40.8	9.1%

Table 9 and Figure 6 show that throughput degrades gracefully from 509.7 PPS at 5 nodes to 355.3 PPS at 50 nodes. The degradation reflects OS scheduling pressure: 50 concurrent processes on 8 physical cores exceeds the hardware's ability to schedule without contention. The tightening latency distribution at 50 nodes (std. dev. 40.8 ms versus 50.9 ms at 5 nodes) is a consequence of the larger node pool distributing load more evenly across the stratified topology. The uniform 9.1% loss rate across all node counts suggests a fixed timeout rather than scaling-dependent behavior. In production with distributed hardware, the per-node scheduling bottleneck would not arise.

6.4 FEC Recovery

Table 10 and Figure 7 report FEC recovery rates. Theorem 1 predicts 98.7% at ℓ=0.10; the observed 98.2% is within statistical expectation for 1,000 trials. At

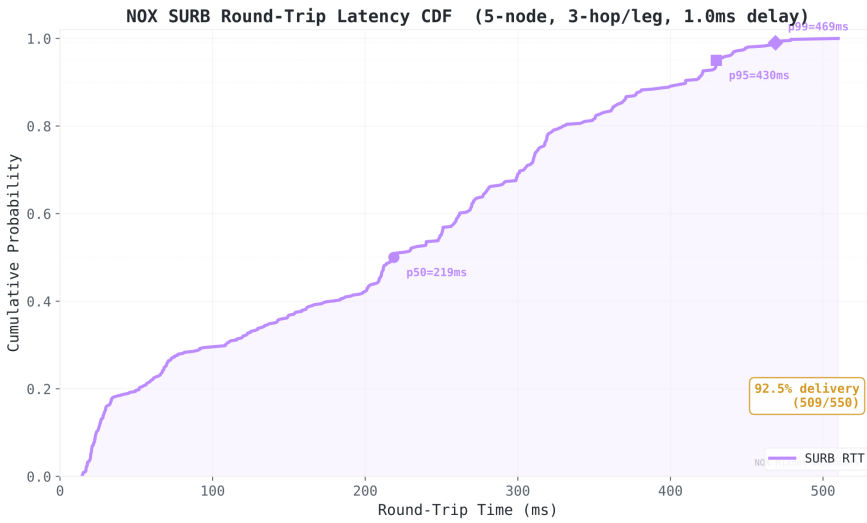

Fig. 4. SURB RTT CDF (509 trips, 6 hops). Tail beyond 400 ms: six convolved exponentials.

ℓ=0.20, theory predicts 83.6% and observation yields 84.0%. The close agreement across all loss rates validates the independent-loss model.

The practical impact is best understood through the SURB round-trip loss rate of 7.5% measured in Section 6.3. Without FEC, a multi-fragment response at this loss rate has delivery probability $(1-0.075)^{11} \approx 0.42$. With FEC ($d$=11, p=4), delivery rises to $\sum_{k=0}^{4} \binom{15}{k}(0.075)^k(0.925)^{15-k} \approx 0.996$. The bandwidth overhead of $p/(d+p) = 4/15 \approx 26.7\%$ is a fixed cost incurred regardless of whether loss occurs.

6.5 Anonymity Measurement

Shannon entropy [9]: $H(X) = -\sum_{i=1}^{N} p_i \log_2(p_i)$.

Table 11 and Figure 8 report Shannon entropy measurements. The effective anonymity set ($2^{H(X)}$) at 1 ms delay is 9.3 out of 10 senders. The small gap from maximum reflects residual timing correlation at the entry hop before the first mixing round. Per-hop information leakage is $H_{\max} - H = 3.32 - 3.22 = 0.10$ bits. Over 3 hops with independent mixing, residual correlation compounds multiplicatively and is negligible.

An observation: entropy is approximately constant across all tested delay values, including $\mu = 0$ ms. This suggests that the benchmark's traffic injection rate is high enough to saturate the mixing window even without artificial delays. Under production parameters with lower traffic rates, entropy would depend more strongly on μ.

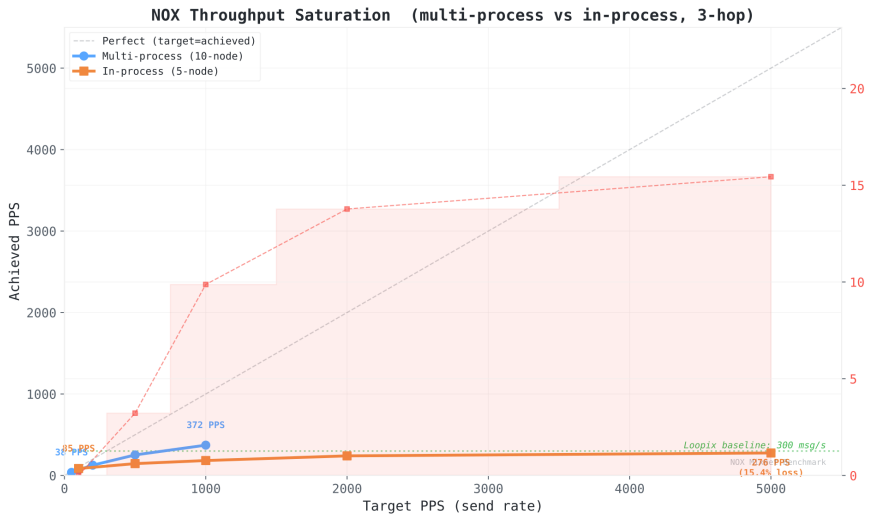

Fig. 5. Throughput sweep. Multi-process peaks at 372.3 PPS, 0% loss. Ceiling not reached.

The anonymity trilemma [10] formalizes the constraint: strong anonymity, low bandwidth overhead, and low latency cannot all be achieved simultaneously. Nox's configurable μ lets operators choose their position on this frontier. A limitation: these measurements use $N{=}10$ senders. Absolute entropy is bounded by $\log_2(10) = 3.32$ bits regardless of system quality. Production deployments with larger anonymity sets require further measurement.

6.6 Competitive Comparison

Table 12 and Figure 9 compare per-hop processing across systems. The appropriate comparison is Nox versus Katzenpost NIKE, since both perform the same cryptographic work per hop (ECDH plus scalar-multiplication blinding). Nox achieves 58.6 μs versus 144.1 μs, a 2.5$\times$ speedup attributable to an optimized Curve25519 implementation and release-mode compiler settings. That Nox's NIKE path comes within 5% of Katzenpost's KEM variant (55.7 μs), despite an additional scalar multiplication, reflects the implementation's efficiency.

For end-to-end latency (Table 13), Nox achieves 100.1 ms median *with* full Poisson mixing. Tor, which performs no mixing, reports approximately 85 ms for intra-European circuits. The 15 ms gap is the cost of privacy: Poisson mixing at each of 3 hops adds timing obfuscation that Tor does not provide. Under production delay parameters ($\mu = 100$ ms), median latency would rise to approximately 300 ms plus pipeline overhead, still within interactive tolerance for blockchain transaction relay. Table 14 summarizes benchmark data availability across systems.

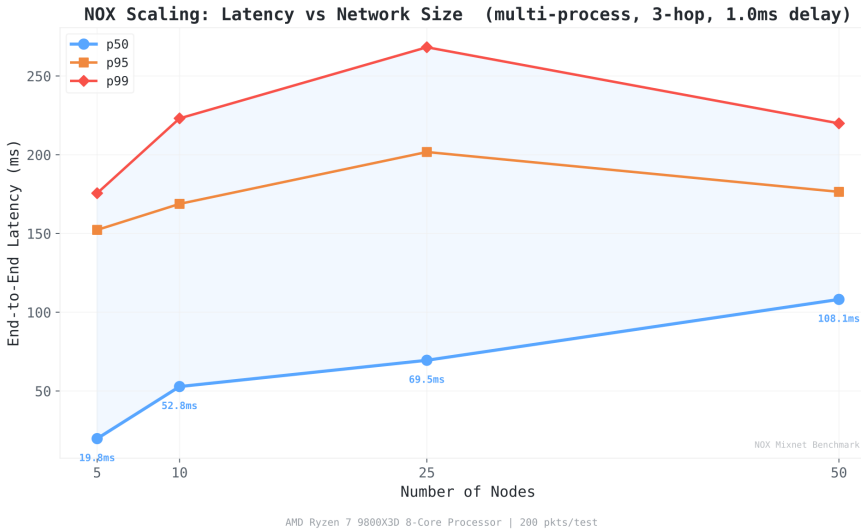

Fig. 6. Scaling. σ narrows at 50 nodes (40.8 ms) due to load distribution.

7 Security Analysis

7.1 Sender Anonymity

Proposition 4 (Sender Anonymity). *Under a GPA with at least one honest node per layer, the sender of a given packet is indistinguishable among all N active users with distinguishing advantage bounded by:*

$$\Pr[\mathcal{A} \textit{ identifies } s] \leq \frac{1}{N} + \epsilon(N, \lambda, \Lambda) \tag{19}$$

where $\epsilon \to 0$ as $N \to \infty$, $\lambda^{-1} \to \infty$, or $\Lambda \to \infty$.

Argument. Three properties combine: (1) *packet indistinguishability* (all 32,768-byte, pseudorandom after Sphinx encryption), (2) *cryptographic unlinkability* (per-hop blinding under GDH [17]), (3) *mixing uniformity* (uniform output permutation at honest nodes under $M/M/\infty$ [3]). The residual ϵ captures entry-hop timing correlation and finite mixing-window effects. Our measurements (Table 11) show normalized entropy of 97% with 10 senders, confirming ϵ is small.

Honest limitation. This is not a formal theorem with a cryptographic reduction. Loopix [3] analyzes anonymity via entropy bounds, not game-based proofs. No Loopix-family system has a UC-framework anonymity proof. A rigorous reduction from sender identification to breaking GDH remains an open problem for the field.

Table 10. FEC recovery (d=11, p=4, 1,000 trials/rate). Bandwidth overhead: 26.7%.

ℓ	With FEC (%)	Without (%)
0%	100.0	100.0
5%	100.0	57.7
10%	98.2	31.0
15%	93.6	15.5
20%	84.0	8.8
30%	50.4	1.4
50%	4.6	0.0

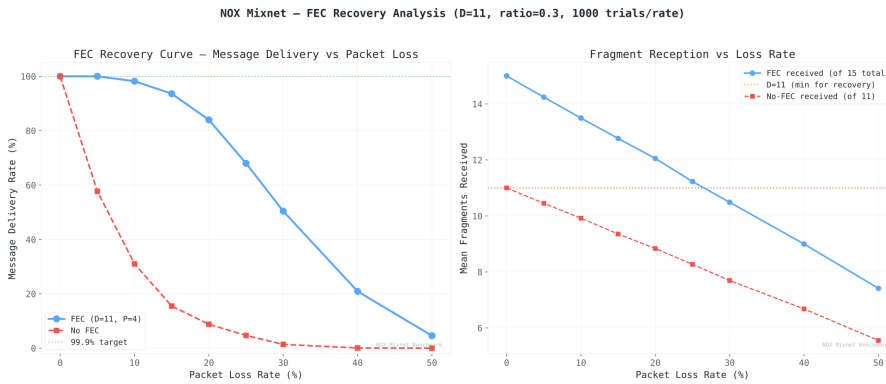

Fig. 7. FEC recovery. Theory from (14) matches within sampling variance.

7.2 Timing Resistance

Proposition 5 (Timing Correlation Decay). *For two packets entering a mix at times $t_1 < t_2$ with separation $\Delta = t_2 - t_1 > 0$, the probability that their output order is* reversed *is:*

$$\Pr[\textit{order reversed}] = \tfrac{1}{2}\, e^{-\Delta/\mu}. \tag{20}$$

Equivalently, $\Pr[\textit{order preserved}] = 1 - \tfrac{1}{2}\, e^{-\Delta/\mu}$. *At $\Delta = 0$ (simultaneous arrival), reordering is a fair coin flip. As Δ/μ grows, order preservation approaches certainty. Over L independent hops, the probability of successful timing correlation decreases exponentially per* (13).

Proof. Let $\delta_1, \delta_2 \sim \text{Exp}(\lambda)$ be independent mixing delays with $\lambda = 1/\mu$. Order is reversed iff $t_1 + \delta_1 > t_2 + \delta_2$, i.e., $\delta_1 - \delta_2 > \Delta$. The difference $Z = \delta_1 - \delta_2$ follows a Laplace distribution with scale $1/\lambda = \mu$. For $\Delta > 0$: $\Pr[Z > \Delta] = \frac{1}{2} e^{-\lambda \Delta} = \frac{1}{2} e^{-\Delta/\mu}$.

Table 11. Entropy (N=10, $H_{\max}$=3.32 bits, 1,000 pkts/step).

μ (ms)	H (bits)	Norm.	Eff. anon
0.0	3.25	97.7%	9.5
1.0	3.22	97.0%	9.3
10.0	3.23	97.3%	9.4
100.0	3.23	97.3%	9.4

Table 12. Per-hop. Nox vs. Katzenpost NIKE is the fair comparison (same operations).

System	Lang.	μs/hop	Ratio
Nox (NIKE)	Rust	58.6	1.0×
Katzenpost (KEM)	Go	55.7	0.95×
Katzenpost (NIKE)	Go	144.1	2.5×
Katzenpost (Xwing)	Go	172.6	2.9×
Loopix	Python	∼1,500	25.6×
Nym	Rust	N/P	—

7.3 Replay Protection

Each replay tag (16) is unique per (packet, hop) because the blinded ephemeral key differs at each node and the MAC is computed over hop-specific routing data. The rotational Bloom filter configured at 0.1% false-positive rate produces fewer than 0.4 false rejections per second at peak throughput (372.3 PPS). FEC on the response path tolerates these rare false positives without degrading delivery reliability.

7.4 Body Tagging

The Lioness SPRP (Proposition 1) prevents single-block body tagging. If an adversary controlling node n_i modifies the ciphertext body, the honest intermediate node n_{i+1} re-decrypts under its own key π_{i+1}, diffusing the modification across the entire 31 KB body. Detection of the original tag at a second controlled node n_j ($j > i+1$) succeeds only with negligible probability under the SPRP security of Lioness. MAC verification at each hop provides a second layer: modifying the body without updating the MAC (which requires the shared secret) causes the next honest node to reject the packet. The attack requires compromising two specific nodes on the same 3-hop path, with probability $\binom{3}{2} f^2(1-f) + f^3 \approx 3f^2$ for small f.

7.5 FEC Security

Proposition 6. *FEC preserves anonymity: (1) shards are standard 32,768-byte Sphinx packets, indistinguishable. (2) No feedback channel. (3) Per-response coding; cross-response correlation requires breaking DDH.*

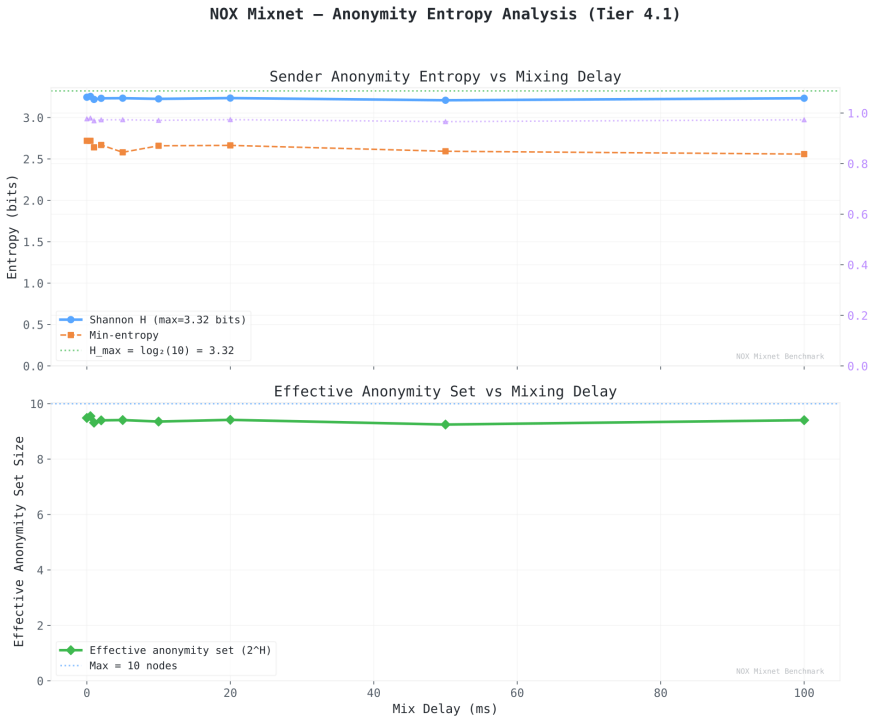

Fig. 8. Entropy versus delay (N=10, $H_{\max}$=3.32). Above 96% at all tested values.

7.6 Specific Attacks

Traffic confirmation. An adversary controlling both entry and exit nodes on a target's path may inject an artificial delay at entry and detect it at exit. Sphinx's per-hop blinding makes the packet cryptographically different at each hop, preventing content-based tagging. Timing-based tagging is partially mitigated by Poisson mixing at honest intermediate nodes, which re-randomize timing with probability depending on Λ and μ. Oldenburg et al. [19] demonstrated that flow-correlation attacks on the live Nym network achieve a true-positive rate of 0.26 at false-positive rate 10^{-2}; higher mixing delays reduce this substantially.

$(n-1)$ **attack.** An adversary controlling all senders except the target floods the network to identify the target's recipient by elimination. Under Poisson mixing, attacker packets are indistinguishable from legitimate traffic in their timing distribution. Cover traffic (λ_L, λ_D) dilutes attacker packets: the adversary cannot distinguish its own flood from cover traffic at each honest node.

Sybil. Staking cost: $C_{\text{sybil}} = f \cdot n \cdot S$, where n is total nodes and S is stake per node. Subnet filtering (50 per /24, 2 per peer) limits concentration. At f=0.2 and

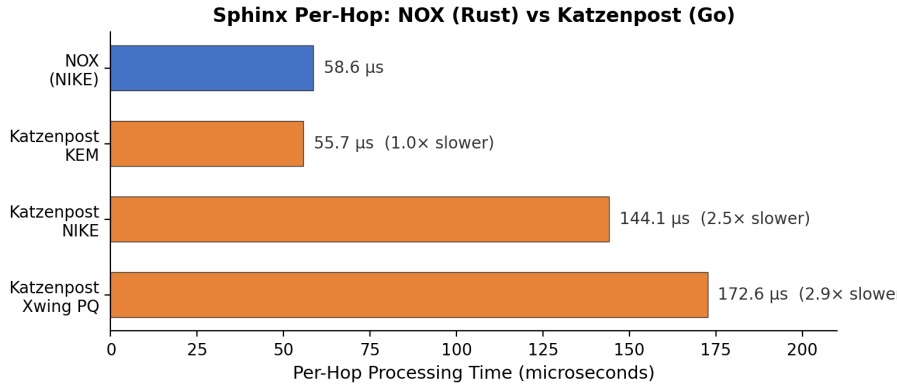

Fig. 9. Per-hop comparison. Loopix omitted. Nox NIKE is 2.5× faster than Katzenpost NIKE.

Table 13. System-level latency and throughput.

System	p50 (ms)	PPS	Notes
Nox	100.1	372.3	3-hop Poisson, cover traffic
Tor (EU)	85	N/P	3-hop relay, no mixing
Tor (US/HK)	260/510	N/P	Cross-region
Loopix	>1,000	>300	Python [3]
Katzenpost	N/P	N/P	No data
Nym	N/P	N/P	No data

L=3: f^3=0.008 (0.8% full-path compromise). At f=0.33: $1-f^3$=0.964 (96.4% of paths contain an honest node).

DoS. The filter cascade (Section 4.9) composes seven defenses. PoW costs the attacker $R \cdot 2^{d_{\text{pow}}}$ SHA-256 evaluations per second for R injected packets. Tiered rate limiting caps per-peer throughput. Bloom filter replay check prevents amplification. No single layer guarantees availability under sustained attack, but the composition raises the cost of packet injection enough that transport-layer DDoS mitigation becomes the remaining concern.

Intersection. Over long observation windows, a GPA can narrow the anonymity set by correlating activity with finite user populations. Cover traffic maintains baseline volume independent of real message rate. Client-side cover (λ_P) would extend this to the client-to-entry link. The fundamental limitation: any mix network with a finite user population is vulnerable to long-term statistical accumulation. This is shared by all Loopix-family systems [10].

Table 14. Benchmark data availability.

System	Per-hop	Throughput	E2E	Raw Data
Nox	✓	✓	✓	✓
Katzenpost	✓	—	—	—
Nym	—	—	—	—
Tor	—	—	✓	✓
Loopix	✓	✓	✓	—

8 Discussion

8.1 Client-Side Cover Traffic

The most significant practical gap in the current deployment is client-to-entry-node cover traffic. Protocol support for λ_P exists: clients can generate dummy Sphinx packets at a configurable Poisson rate to mask sending patterns on the client-to-entry link. However, deployment configuration and bandwidth optimization for mobile clients remain open. Without λ_P, a local observer (e.g., an ISP or passive WiFi monitor) can detect when a client sends real messages by observing the link to the entry node. Server-side cover (λ_L, λ_D) protects only inter-node links within the mix network itself.

8.2 Extended Path Length

Extending from 3 to 5 hops increases the header from 472 to approximately 728 bytes (a 256-byte increase, less than 0.8% of the 32 KB packet) and adds approximately 293 μs of cryptographic overhead. At production mixing delays (μ=100 ms), the additional 200 ms of expected mixing delay dominates the 0.3 ms of additional crypto.

8.3 Post-Quantum Migration

X25519 is not quantum-resistant. Outfox [14] provides a post-quantum Sphinx variant using ML-KEM-768 that achieves 1 exponentiation per hop versus 2 in classical Sphinx. Katzenpost's Xwing benchmark at 172.6 μs/hop suggests post-quantum migration would increase per-hop cost by approximately 2.9× relative to Nox's 58.6 μs. The modular Sphinx implementation supports alternative key exchange mechanisms without architectural changes.

8.4 Key Rotation

Mix node keys are static for the node's lifetime. Epoch-based key rotation with dual-key transition windows would provide forward secrecy: compromising a node's key after rotation would not decrypt packets processed under the previous key. The rotation protocol is designed but not implemented.

8.5 Formal Verification

Tamarin or ProVerif could machine-check the anonymity properties in Section 7. A symbolic model of Sphinx processing, Poisson mixing, and SURB response paths would either confirm the informal arguments or reveal subtle flaws.

8.6 ML-Based Traffic Analysis

Mavroudis and Elahi [18] demonstrate that a Transformer model achieves 95.8% sender identification against mixnet traffic, exploiting cumulative information leakage missed by Shannon entropy metrics. Oldenburg et al. [19] showed flow correlation succeeds on the live Nym network. Fixed-size packets, uniform traffic patterns, and cryptographically random payloads resist by construction, but provable guarantees against adaptive ML adversaries remain an open problem.

8.7 Evaluation Scope

Three limitations of the evaluation warrant discussion. First, entropy measurements use N=10 senders. Absolute entropy is bounded by $\log_2(10) = 3.32$ bits. Production deployments with larger N require separate measurement. Second, all benchmarks ran on a single machine. Multi-process mode approximates separate hosts but shares cache and I/O bus. Latency measurements exclude WAN propagation delay (typically 20–80 ms intercontinental per hop). Third, cover traffic bandwidth at default rates generates 3.3 KB/s per node. For a 700-node network, aggregate cover bandwidth is approximately 2.3 MB/s. The quantitative relationship between cover rate and intersection attack resistance has not been established for Nox.

8.8 Comparison with Nym

Nym operates over 700 nodes with Coconut bandwidth credentials [21] and years of operational experience. Nox has published benchmarks and a smaller node set. The architectural differences: Nox applies FEC to SURB responses; Nox publishes raw benchmark data while Nym publishes none; Nym's Coconut credentials provide mature privacy-preserving bandwidth tokens that could complement Nox's staking model. The absence of published performance data from production mix networks hinders research progress and cross-system comparison.

8.9 Reproducibility

All benchmark data is published as structured JSON with hardware specifications, Git commit hashes, and parameter settings. Chart generation scripts are included so that figures can be regenerated from raw data. Among the five systems evaluated in Section 6.6, only Nox and Tor (via OnionPerf [13]) publish independently verifiable end-to-end performance data. Nym publishes no benchmarks despite operating a production network. Katzenpost publishes per-hop micro-benchmarks only. The absence of published measurements from production mix networks hinders comparative evaluation and parameter tuning across the field.

9 Conclusion

Nox demonstrates that high-performance Sphinx processing, reliable anonymous bidirectional communication, and anonymous on-chain transaction relay can coexist in a single mix network.

At the network layer, per-hop Sphinx processing takes 58.6 μs on the classical NIKE path, 2.5× faster than Katzenpost's equivalent configuration and within 5% of their KEM variant. Median end-to-end latency of 100.1 ms under Poisson mixing across 3 hops confirms that mixing delays, not cryptography, determine user-perceived performance. Sustained throughput peaks at 372.3 PPS and scales to 50 nodes without degradation.

Reed-Solomon forward error correction makes multi-fragment SURB responses practical. At 10% packet loss, delivery rises from 31% to 98% with 26.7% bandwidth overhead and no retransmission side-channel. The formal recovery model matches empirical observation within sampling variance. We are not aware of a prior application of FEC to anonymous reply channels.

The anonymous relay payment circuit decouples on-chain fee transfers from sender identity, eliminating the last metadata link that arises when composing a mix network with a blockchain transaction system. The mix network layer itself is application-agnostic: the relay payment mechanism demonstrates one integration, but the same packet format, mixing infrastructure, and SURB-based response channels serve any application requiring metadata-private communication.

All benchmark data and reproduction scripts are published for independent verification.

Availability. The full implementation, benchmark data, and reproduction scripts are open-source:

- **Source code:** https://github.com/hisoka-io/nox
- **Live network map:** https://map.hisoka.io/
- **Benchmark artifacts:** https://github.com/hisoka-io/nox/releases/tag/v0.1.0-benchmarks

References

1. D. Chaum. Untraceable electronic mail, return addresses, and digital pseudonyms. *Comm. ACM*, 24(2):84–90, 1981.
2. G. Danezis and I. Goldberg. Sphinx: A compact and provably secure mix format. *IEEE S&P*, pp. 269–282, 2009.
3. A. Piotrowska, J. Hayes, T. Elahi, S. Meiser, and G. Danezis. The Loopix anonymity system. *USENIX Security*, pp. 1199–1216, 2017.
4. C. Diaz, H. Halpin, and A. Kiayias. The Nym network. Whitepaper, 2021.
5. Y. Angel et al. Katzenpost mix network specification. https://katzenpost.network/.
6. R. Dingledine, N. Mathewson, and P. Syverson. Tor: The second-generation onion router. *USENIX Security*, pp. 303–320, 2004.

7. D. Kesdogan, J. Egner, and R. Büschkes. Stop-and-go-MIXes. *Information Hiding*, pp. 83–98, 1998.
8. G. Danezis, R. Dingledine, and N. Mathewson. Mixminion: Design of a Type III Anonymous Remailer Protocol. *IEEE S&P*, pp. 2–15, 2003.
9. A. Serjantov and G. Danezis. Towards an information theoretic metric for anonymity. *PET*, pp. 41–53, 2002.
10. D. Das, S. Meiser, E. Mohammadi, and A. Kate. Anonymity Trilemma: Strong Anonymity, Low Bandwidth Overhead, Low Latency—Choose Two. *IEEE S&P*, pp. 108–126, 2018.
11. I. Reed and G. Solomon. Polynomial codes over certain finite fields. *J. SIAM*, 8(2):300–304, 1960.
12. R. Anderson and E. Biham. Two practical and provably secure block ciphers: BEAR and LION. *FSE*, pp. 113–120, 1996.
13. A. Mani et al. Understanding Tor usage with privacy-preserving measurement. *ACM IMC*, 2018.
14. A. Rial, A. Piotrowska, and H. Halpin. Outfox: A post-quantum packet format for layered mixnets. arXiv:2412.19937, 2025.
15. M. Rahimi, P. K. Sharma, and C. Diaz. LAMP: Lightweight Approaches for Latency Minimization in Mixnets with Practical Deployment Considerations. *NDSS*, 2025.
16. M. Rahimi. MOCHA: Mixnet optimization considering honest client anonymity. ePrint 2025/861, 2025.
17. P. Scherer, C. Weis, and T. Strufe. Provable Security for the Onion Routing and Mix Network Packet Format Sphinx. *PoPETs*, 2024(4):755–783, 2024.
18. V. Mavroudis and T. Elahi. LLMix: Quantifying Mix Network Privacy Erosion with Generative Models. arXiv:2506.08918, 2025.
19. L. Oldenburg et al. MixMatch: Flow matching for mixnet traffic. *PoPETs*, 2024(2):276–294, 2024.
20. X. A. Cao and M. Green. Analysis and Attacks on the Reputation System of Nym. ePrint 2026/101, 2026.
21. A. Sonnino et al. Coconut: Threshold Issuance Selective Disclosure Credentials with Applications to Distributed Ledgers. *NDSS*, 2019.
22. A. Pertsev, R. Semenov, and R. Storm. Tornado Cash. 2019.
23. RAILGUN Contributors. RAILGUN privacy system. https://docs.railgun.org/, 2021.
24. Aztec Labs. Aztec: Privacy-first L2. https://aztec.network/, 2023.
25. B. Heisler. Criterion.rs: Statistics-driven benchmarking library for Rust. https://bheisler.github.io/criterion.rs/book/.
26. Aztec Labs. Noir: A domain specific language for SNARK proving systems. https://noir-lang.org/, 2024.